# Scaled-energy spectroscopy of helium $|M|=1$ Rydberg atoms in a static electric field

Annemieke Kips, Wim Vassen, and Wim Hogervorst
*Department of Physics and Astronomy, Vrije Universiteit, De Boelelaan 1081, 1081 HV Amsterdam, The Netherlands*

Paul A. Dando
*Department of Physics and Astronomy, University College London, Gower Street, London WC1E 6BT, United Kingdom*
(Received 8 May 1998)

We present scaled-energy spectra on helium Rydberg atoms in a static electric field. $|M|=1$ states were studied in excitation from the $2\,^1S_0$ metastable state. Spectra were recorded for $\epsilon=-2.940(4)$, $\epsilon=-2.350(4)$, both below the saddle point, and $\epsilon=-1.760(4)$, above the saddle point. Closed-orbit theory was applied to interpret the spectra. A recent extension to closed-orbit theory, incorporating core effects, was used. This significantly improved agreement between experiment and theory. [S1050-2947(98)02610-9]

PACS number(s): 32.60.+i, 32.80.Rm, 03.65.Sq

## I. INTRODUCTION

In this paper we present high-resolution laser spectroscopy experiments on helium Rydberg atoms in a static electric field. In an electric field the classical Hamiltonian of a hydrogen atom may be transformed in such a way that it does not depend on energy and applied field independently but solely on a single parameter: the scaled energy $\epsilon=E/\sqrt{F}$. Here $E$ is the energy with respect to the zero-field ionization threshold and $F$ is the applied electric field, both in atomic units. This scaling property has inspired experimentalists to perform experiments under constant semiclassical conditions by varying the electric-field strength and energy simultaneously in such a way that the scaled energy is kept constant. In this way the classical dynamics of the atom does not change during a laser scan and semiclassical closed-orbit theory can be applied to interpret the spectra. This theory, developed by Delos and co-workers [1–3], connects the oscillations in the absorption spectra of a hydrogen atom in an external field to classical electron orbits that are closed at the nucleus. Such a semiclassical description of a quantum system is attractive since, in contrast to a full quantum calculation, it can provide greater insight into the dynamics.

To date, most theoretical and experimental work on scaled-energy spectroscopy has been performed on atoms in magnetic fields since, in this case, a transition from regular to chaotic classical dynamics can be studied when increasing the scaled energy. The hydrogen atom in an electric field, on the other hand, is an integrable system and hence no such transition to chaos exists. However, for nonhydrogenic atoms, the presence of a core induces additional scattering possibilities that may be interpreted as chaotic behavior, in both the electric- and magnetic-field cases. Therefore, these core-induced effects may be equally well studied in an electric field. Additionally, the Coulomb plus electric-field potential contains a saddle point. When the energy is higher than the saddle point energy (corresponding to $\epsilon>-2$) a classical electron can escape into the continuum. A study at energies around the saddle point energy in the electric-field case offers additional attractive features.

A scaled-energy experiment in an electric field was performed by Eichmann *et al.* [4] on sodium at $\epsilon=-2.5$. Spectra were recorded in pulsed-laser excitation and compared with hydrogenic closed-orbit calculations. In these calculations so-called action spectra were generated and compared with Fourier transforms of the experimental spectra. Due to their limited energy resolution, the experiments were restricted to small-scaled actions ($\tilde{S}<10$). Courtney *et al.* [5] recorded scaled-energy spectra for lithium ($M=0$) at various scaled energies below and above the saddle point using two-step cw laser excitation. Orbits born from bifurcations from the parallel orbit and its repetitions were studied as a function of the scaled energy. These spectra were also interpreted using closed-orbit theory. Large deviations in the intensities of the peaks of Fourier transformed experimental spectra from hydrogenic closed-orbit calculations were found, in particular for higher action values. Some of these could be attributed to core effects. Kuik *et al.* [6] performed scaled-energy experiments on barium Rydberg atoms in an electric field. Their spectra were also interpreted using hydrogenic closed-orbit theory. Effects of the nonhydrogenic character of barium were observed as deviations (mainly in the intensities of the peaks) from hydrogenic closed-orbit calculations.

In early versions of closed-orbit theory core scattering was ignored. Gao and Delos [3] considered core scattering and demonstrated that an incoming Coulomb wave at the core is not only scattered backward into its own orbit but is also scattered into all other orbits. However, the effects were expected to be small for the system they were studying and were neglected. Over the past few years both theoretical and experimental evidence have been collected, showing that effects of the core in nonhydrogenic atoms cannot be neglected in general [5,7,9,10]. In the Fourier transforms of experimental spectra and of quantum calculations, additional peaks and a reduction of intensities of the hydrogenic modulations and their harmonics were found. To describe the effects of a nonhydrogenic core in semiclassical calculations two approaches have been used. Dando *et al.* [11,12] investigated the scattering of an incoming Coulomb wave at the core in detail and demonstrated that incorporating the core-scattered waves consistently in closed-orbit theory results in the appearance of sum orbits, whose scaled action is the sum of the actions of two or more hydrogenic orbits. These ''combina-

 

tion'' orbits were first identified in magnetic-field experiments [7]. Also the probability for repeated traversals of hydrogenic orbits is reduced as part of the amplitude of the incoming wave may be scattered into other orbits, a process termed ''core shadowing.'' An alternative approach employed by Hüpper *et al.* [13,14] accounted for the core in the classical trajectory calculations via a model potential constructed to give the correct quantum defects. Both approaches were successful in comparing modified semiclassical calculations and quantum calculations for highly excited atoms in a magnetic field. The essential difference between the two approaches is that Dando *et al.* describe core-scattering quantum mechanically, while Hüpper *et al.* use a classical treatment. In this paper we apply the description of Dando *et al.*, who achieved excellent agreement between calculated quantum spectra for lithium in an electric field at $\epsilon = -3.00$ and their modified closed-orbit theory calculations.

Here we present $|M|=1$ spectra for singlet helium at $\epsilon = -2.940(4)$, $\epsilon = -2.350(4)$, both below the saddle point, and $\epsilon = -1.760(4)$, which is above the saddle point. We compare our experimental data with hydrogenic closed-orbit theory and show how the results improve on including core effects in the way described by Dando *et al.* [11,12]. Since orbits along the electric field direction are not present for $|M|=1$ spectra, corrections for diverging amplitudes [15] close to bifurcations are not necessary. We also estimate whether the possibility of escape over the saddle point after core scattering affects the spectra significantly. Since helium has a small core its core effects are expected to be small, but they are incorporated in our calculations. We chose to study helium following experiments on barium performed in our group by Kuik *et al.* [6]. In contrast to barium, helium is theoretically better accessible. For helium, quantum spectra can be calculated with high accuracy and due to its small quantum defects the experimental spectra are expected to deviate only slightly from hydrogenic closed-orbit theory calculations. The experiments on helium presented here are more pure than those previously performed on barium. Since helium has a $J=0$, $M=0$ metastable state either $M=0$ or $|M|=1$ states can be excited, depending on the polarization of the laser with respect to the electric-field direction. To allow single-step excitation to the zero-field ionization limit, as done by Kuik *et al.*, barium atoms were also excited from a metastable state. Barium metastable states have $J\neq 0$ and therefore the spectra contained contributions from several $M$ values simultaneously. We chose to study singlet helium at the scaled-energy values mentioned above to allow for future comparison with previously recorded barium spectra at the same scaled energies.

The paper is organized as follows. In Sec. II we briefly review the theoretical ideas underlying scaled-energy spectroscopy, closed-orbit theory, the modifications suggested by Dando *et al.* to incorporate the effects of a core in nonhydrogenic atoms, and the properties of helium specific to this experiment. In Sec. III the experimental setup and the calibration procedure are discussed. In Sec. IV an interpretation of the experiments using closed-orbit theory is given. The paper ends with some conclusions in Sec. V.

## II. THEORY

### A. Scaled-energy spectroscopy

In our experiment we use the technique of scaled-energy spectroscopy in which the frequency of the laser and the applied electric field are varied simultaneously. This experimental technique is based on a scaling property of the Hamiltonian $H_F$ for a hydrogen atom in an electric field:

$$H_F=\frac{1}{2}(p_z^2+p_\rho^2+l_z^2/\rho^2)-1/(\rho^2+z^2)^{1/2}+Fz. \tag{1}$$

Here $\rho^2=x^2+y^2$, $F$ is the applied electric field in atomic units, and $l_z$ is the $z$ component of the angular momentum. Inserting the transformation

$$\begin{aligned} \tilde{\rho}&=F^{1/2}\rho, \quad \tilde{p}_\rho=F^{-1/4}p_\rho, \\ \tilde{z}&=F^{1/2}z, \quad \tilde{p}_z=F^{-1/4}p_z, \quad \tilde{t}=F^{3/4}t \end{aligned} \tag{2}$$

results in a scaled Hamiltonian $\tilde{H}$,

$$\tilde{H}=H_F/\sqrt{F}=\frac{1}{2}(\tilde{p}_z^{\,2}+\tilde{p}_\rho^{\,2}+L_z^2/\tilde{\rho}^{\,2})-1/(\tilde{\rho}^{\,2}+\tilde{z}^{\,2})^{1/2}+\tilde{z}, \tag{3}$$

with $L_z=F^{1/4}l_z$.

When considering the classical dynamics of the system in scaled coordinates we find that for $L_z=0$ there is no longer a separate dependence on the electric field and energy. The classical dynamics is completely determined by a single parameter, the scaled energy

$$\epsilon=E/\sqrt{F}. \tag{4}$$

The scaling property of the electric field Hamiltonian allows for absorption experiments under constant semiclassical conditions provided the scaled energy is kept constant.

In our experiment $l_z=1$. For $l_z=1$ the scaling property of the Hamiltonian is only approximate since $L_z$ still depends on the applied electric field. However, in our experiments $F^{1/4}\simeq 1/150$, which implies that the centrifugal term in the scaled Hamiltonian is two orders of magnitude smaller than the other terms, making $l_z=0$ a good approximation.

### B. Closed-orbit theory

Our experimental data were interpreted using the semiclassical closed-orbit theory developed by Delos and coworkers [1–3]. This theory has been described in great detail in several papers; here we will only give a brief summary of this theory as well as the basic equations. The near-threshold absorption spectrum of an atom in an external field consists of a series of (deformed) sinusoidal oscillations superimposed on a slowly varying background. Closed-orbit theory connects each oscillation to a classical electron orbit that is closed at the nucleus. Two different regions in space are distinguished: the region near the core ($r<r_b$, $r_b\sim 50a_0$), where a quantum description is required, and the region far away from the core ($r>r_b$), where a semiclassical description is feasible.

In closed-orbit theory the absorption of a photon by an atom in an external field excites an electron that leaves the core region in an (almost) zero-energy outgoing Coulomb wave at an initial launching angle $\theta_{\text{initial}}$ to the field direction. For $r>r_b$, this wave propagates semiclassically; the electron follows a classical trajectory and its dynamics is governed by

Hamilton's equations of motion. Eventually, the trajectory will curve back in the combined Coulomb–electric-field potential. The electron may then return to the core, its trajectory making an angle $\theta_{\text{final}}$ with the field direction. Here again a quantum description is needed and a scattering wave function can be constructed. An electron orbit that closes exactly at the core results in an oscillation in the absorption spectrum as a consequence of interference between the returning wave scattering at the core and the original outgoing wave. In an absorption experiment the average oscillator strength distribution $f$ is measured, which consists of a slowly varying background $f_0$ together with an oscillatory part $f_1$ involving a sum of contributions over all closed orbits $j$ of the system:

$$f_1=[-2(E-E_i)/\pi]\,\mathrm{Im}\sum_j N_j\langle D\Psi_i|\Psi_{\text{return}}\rangle. \tag{5}$$

Here $E-E_i$ is the energy of the electron with respect to the zero-field ionization limit of the atom $E_i$, $\Psi_i$ is the wave function of the initial state from which the laser excitation occurs, $D$ is the component of the dipole operator relevant for the polarization of the exciting laser, and $\Psi_{\text{return}}$ is the wave function of the returning wave scattered at the core.

The coefficients $N_j$ are calculated by matching the semiclassical wave returning to the core with the incoming part of the scattered wave function $\Psi_{\text{inc}}(r_b,\theta^j_{\text{final}})$ at the boundary $r=r_b$. The resulting matching equation, with the semiclassical approximation on the left-hand side, is

$$\Phi_{\text{initial}}(r_b,\theta^j_{\text{initial}})A_j e^{i(S_j+\phi_j)}=N_j\Psi_{\text{inc}}(r_b,\theta^j_{\text{final}}), \tag{6}$$

where $S_j$ is the classical action of the electron built up along its trajectory back to the core, $\phi_j$ is an additional phase term, $A_j$ is an amplitude related to the stability of the orbit, and $\Phi_{\text{initial}}(r_b,\theta^j_{\text{initial}})$ is the initial outgoing wave function at $r=r_b$ needed to construct the semiclassical wave function.

In the case of hydrogen, the initial outgoing Coulomb wave at the boundary between the semiclassical and quantum region is used as a starting condition for constructing the semiclassical wave:

$$\Phi_{\text{initial}}(r_b,\theta^j_{\text{initial}})=\Phi_{\text{out}}(r_b,\theta^j_{\text{initial}}). \tag{7}$$

The calculated $N_j$ is then proportional to $A_j e^{iS_j}$. The $j$th closed orbit thus leads to an oscillation with frequency $S_j$ and amplitude $A_j$ in the absorption spectrum. Coulomb scattering is focused strongly backward and may result in repeated traversals of the orbit. These are connected to harmonics in the oscillator strength distribution.

For a nonhydrogenic atom, the initial outgoing wave needs correction. In this case, the scattered quantum wave function consists not only of an incoming part returning to the core and a Coulomb part scattered back in the direction of the incoming trajectory but also of an additional outgoing, core-scattered wave

$$\Psi_{\text{return}}(r,\theta)=\Psi_{\text{inc}}(r,\theta)+\Psi_{\text{Coulomb}}(r,\theta)+\Psi_{\text{core}}(r,\theta). \tag{8}$$

The effect of the core-scattered waves is to redistribute amplitude into all other closed orbits. In this way the probability that after traveling along any closed orbit the electron is scattered by the core into another closed orbit is accounted for.

To incorporate the effect of the core-scattered waves in the closed-orbit sum, the extra outgoing waves have to be added to the starting condition for constructing the semiclassical wave function [11]

$$\Phi_{\text{initial}}(r_b,\theta^j_{\text{initial}})=\Phi_{\text{out}}(r_b,\theta^j_{\text{initial}})+\sum_k N_k\Psi^k_{\text{core}}(r_b,\theta^j_{\text{initial}}). \tag{9}$$

On substituting this expression for $\Phi_{\text{initial}}$ into Eq. (6) and introducing scaled coordinates, we arrive at the expression for $N_j$ given in Ref. [12]:

$$N_j=\left[D_j(\theta^j_{\text{initial}})+\sum_{k,p}N_k B^{k,p}_j(\theta^j_{\text{initial}})\right]\sum_n \hbar_{\text{eff}}^{\nu_j/2}A^n_j e^{i\Delta^n_j}. \tag{10}$$

The first term on the right-hand side of Eq. (10) accounts for the oscillation due to the hydrogenic orbit $j$. The second term accounts for all sum orbits for which the electron is finally core scattered from an orbit $k$ into the orbit $j$. The harmonics of $j$ and $k$ are labeled by $n$ and $p$, respectively. The index $\nu_j$ is 2 for orbits with $\theta^j_{\text{initial}}=0°$ or 180° and 1 for all other orbits. The value of the effective Planck constant $\hbar_{\text{eff}}$ can be deduced easily from the commutation relation between position and momentum operators in scaled coordinates. As $\hbar_{\text{eff}}$ decreases the system becomes more classical and core effects become less pronounced.

The resulting matching equation (10) now has $N$ values on both sides and is most conveniently solved by an iterative procedure. We begin by setting $N_k$ on the right-hand side of Eq. (10) to zero and obtain a first approximation to $N_j$; this is equivalent to the hydrogenic closed-orbit result. In each successive step extra terms of the form $A_k\cdots A_j e^{i(S_k+\cdots+S_j)}$ are added to the previous result. These terms lead to an extra class of orbits in the nonhydrogenic system: sum orbits. They are combinations of two or more hydrogenic orbits and have a classical action that is the sum of the classical actions of the hydrogenic orbits involved. In successive steps of the iterative process combinations of more and more orbits are included. From Eq. (10) we see that each successive term in the iterative process scales as $\hbar_{\text{eff}}^{\nu_j/2}$ ($\hbar_{\text{eff}}=F^{1/4}$) and so the iterative procedure converges rapidly for sufficiently small $\hbar_{\text{eff}}^{\nu_j/2}$ provided we are away from bifurcations where the semiclassical amplitude is infinite. In addition, a change in the contribution to the harmonics of hydrogenic orbits, which arise due to the Coulomb scattering, can also be expected as a result of core scattering.

One of the experimental recurrence spectra we present in this paper is at a scaled energy above the saddle point. Above the saddle point launching angles for the electron exist for which it will escape into the continuum. These electrons do not return to the core and therefore do not affect the recurrence spectrum. There is also a finite possibility that an electron, after traveling once along a closed trajectory, can, upon returning to the core region, be scattered such that it can escape over the saddle point. This will occur when the initial angle with the applied electric field direction is larger than $\alpha(\epsilon)$ [$\alpha(\epsilon=-1.76)=120°$]. When the probability that

the electron upon return is core scattered over the saddle point into the continuum is significant, the contributions of its harmonics and of sum orbits involving this orbit will be affected. However, here we present spectra of $|M|=1$ states. In these spectra we only see effects of the quantum defects of series with orbital angular momenta $l \geqslant 1$, which are small for helium singlets. Furthermore, the dominant term in the core-scattered part of the returning wave function is proportional to $Y_{1,\pm 1}(\theta)$ and is small for large $\theta$. Therefore, we expect that this escape process will not affect our spectra significantly and, for this reason, it is not included in our calculations.

Closed orbits were found by varying the initial launch angle of the electron with the electric-field direction between 0° and 180° in steps of 0.001°. After launching the electron from the core, its motion is calculated by integrating Hamilton's equations of motion. The integration is performed in parabolic coordinates to circumvent the Coulomb singularity at the core:

$$u=\sqrt{(\tilde{r}+\tilde{z})}, \quad v=\sqrt{(\tilde{r}-\tilde{z})}. \tag{11}$$

It is convenient to use the $l_z=0$ potential in the classical region. The scaled $l_z=1$ potential-energy surface differs from the scaled $l_z=0$ surface only close to the $z$ axis. An orbit with $l_z=1$ cannot cross the centrifugal barrier at the $z$ axis, but is reflected at this barrier instead. The scaled actions of the $l_z=1$ orbits are expected to differ only slightly from their $l_z=0$ counterparts since most of the time the electron travels far away from this centrifugal barrier. This is especially true for the strongest features in the $l_z=1$ spectra, which originate from orbits that leave the core region almost perpendicularly to the $z$ axis, that is, along the $\rho$ axis. The phase change associated with a crossing of the $z$ axis is the same as for reflection at the centrifugal barrier. We reconstruct spectra in the $F^{-1/4}$ range relevant for the experiment by superimposing the oscillations with their amplitudes, actions, and additional phases, which result from the closed orbits. We then use a Fourier transform routine to obtain recurrence spectra that can be compared with Fourier transforms of our experimental spectra. A sine window was used to reduce the spurious oscillations due to cutoff effects observed when a rectangular window is used.

### C. Helium

Rydberg states of the two-electron helium atom can be described by the relatively simple atomic physics of a one-electron system. Its singlet and triplet states belong to two strictly separated systems. The experiments presented in this paper were performed on the singlet system. Since we studied $|M|=1$ states, only quantum defects of states with $l \geqslant 1$ have to be considered. The helium core is incorporated in the theory using the following values for the singlet quantum defects: $\mu(l=1)=-0.011\,95$, $\mu(l=2)=0.002\,111$, $\mu(l=3)=0.000\,438$, $\mu(l=4)=0.000\,125$, $\mu(l=5)=0.000\,048$, $\mu(l=6)=0.000\,017$, and $\mu(l>6)=0.0$. For our experiments $Y(\theta)$, which determines the angular distribution of the initially outgoing wave and is connected to the initial state and the polarization of the laser, is

$$Y(\theta)=-Y_{1,\pm 1}(\theta)=\sin\,\theta. \tag{12}$$

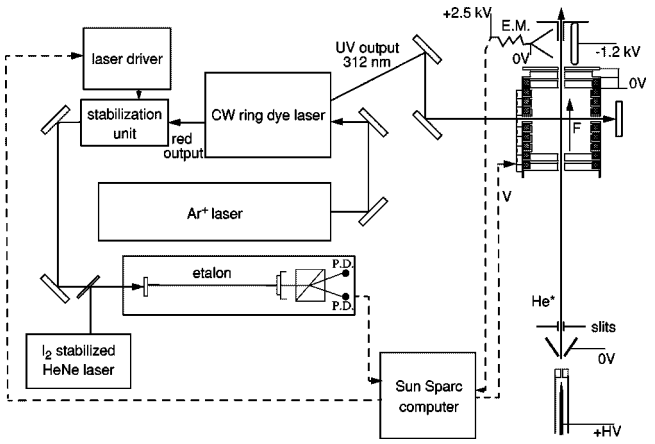


FIG. 1. Schematic drawing of the experimental setup. E.M. denotes the electron multiplier and P.D. denotes the photodiode.

## III. EXPERIMENT

In Fig. 1 a schematic diagram of the experimental setup is shown. Excitation starts from the $1s2s\ ^1S_0$ metastable state. An atomic beam is formed by expanding helium gas out of a quartz tube through a boron nitride nozzle. The expanding gas is collimated by a skimmer and a horizontal and vertical slit pair. The $1s2s\ ^1S_0$ metastable state is populated in a discharge running between a stainless steel needle inside the quartz tube at a negative high voltage and the grounded skimmer. In the interaction region the atomic beam is perpendicularly intersected by the UV output ($\sim$8 mW, 312 nm) of an intracavity frequency doubled rhodamine-B cw ring dye laser (Spectra Physics 380D) containing a 2-mm-thick Brewster cut $LiIO_3$ crystal. The dye laser is pumped by an $Ar^+$ laser (Spectra Physics 2045). $1snp\ ^1P_1$ Rydberg states are excited from this metastable state in a single step.

The interaction region is located inside a small stainless steel box. Further downstream excited Rydberg atoms are field ionized underneath a channeltron electron multiplier, which counts the detached electrons. Signals of this electron multiplier are stored on a Sun Sparc computer, which also controls the experiment. The interaction region is built up of a series of metal rings isolated from each other by ceramic spacers. To apply the electric field a voltage difference is set over the outermost rings (separation $\sim$2.25 cm). The voltage is evenly distributed over the rings by a chain of resistors. This eliminates boundary effects and results in a more homogeneous field. In this way a field is applied along the atomic beam direction. The field direction is chosen such that electrons detached from Rydberg atoms that do not survive the interaction region are pushed out towards the electron multiplier.

It is essential for the experiment that the scaled energy is kept constant during a laser scan of about 40 GHz in the UV. Since the scaled energy depends on laser frequency and applied electric field, the frequency must be known accurately to allow the correct adjustment of the electric field. This requires on-line frequency calibration. Therefore, each laser scan starts by recording a zero-field transition for which the energy is accurately known before switching on the field. The simultaneously recorded transmission of the red output of the dye laser through a 150-MHz length-stabilized confocal étalon is used for further calibration with respect to the

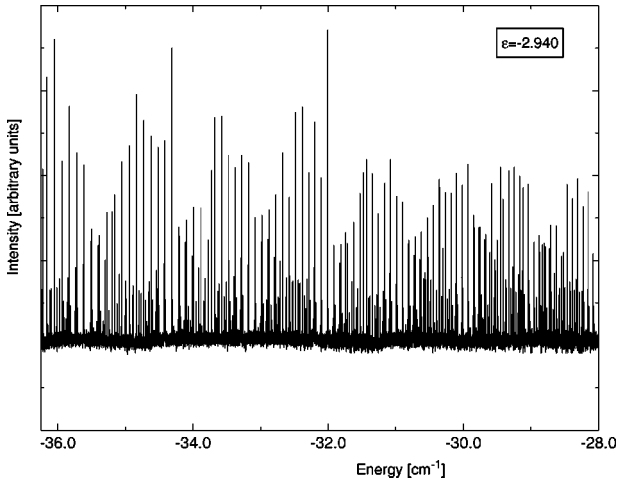


FIG. 2. Experimental spectrum at $\epsilon=-2.940(4)$.

zero-field transition and for adjustment of the applied electric field.

The field is accurately calibrated with the $n=40$ electric-field angular momentum manifolds. The error in the electric field is the major error source for the scaled energy. From the error in the calibration, from the field inhomogeneity deduced from recorded $n=60$ manifolds, and from the remaining stray electric field, an uncertainty in the scaled energy value of 0.004 results.

The laser is polarized perpendicular to the field direction so as to induce $\Delta M=\pm 1$ transitions. $\Delta M=0$ transitions are at least a factor of 200 weaker.

The setup is tested by comparing an experimental spectrum at $\epsilon=-3$ with a calculated quantum spectrum [8]. The results are in good agreement to within the error margins. The calculation showing the best agreement with experiment pinpoints the scaled energy value to within a remaining uncertainty of 0.001. From this the scaled energy within a laser scan is estimated to be constant within 0.001.

We performed experiments at $\epsilon=-2.940(4)$, $\epsilon=-2.350(4)$, both below the saddle point, and $\epsilon=-1.760(4)$, which is above the saddle point. We scanned the energy region in between the $n=55$ and $n=80$ zero-field levels. The lower-$n$ value relates to the highest electric-field strength of 20 V/cm in the present experiment. For $n>80$ small remaining stray electric fields and field inhomogeneities start to become problematic and therefore $n=80$ was an upper limit. The investigated energy range was sufficiently large for a good resolution in the Fourier transformed spectra. We recorded up to 12 overlapping scans, which were then combined and Fourier transformed with respect to $F^{-1/4}$.

## IV. INTERPRETATION OF THE EXPERIMENTAL DATA

### A. Experimental results

We recorded scaled energy spectra for singlet helium at $\epsilon=-2.940(4)$ $(133<F^{-1/4}<151)$, $\epsilon=-2.350(4)$ $(128<F^{-1/4}<157)$, and $\epsilon=-1.760(4)$ $(131<F^{-1/4}<156)$. In Fig. 2 a recording of the experimental spectrum at $\epsilon=-2.940(4)$ is shown. At this scaled energy it appears that the spectrum consists of overlapping $|M|=1$ Stark manifolds of adjacent $n$ values. The strongest and narrowest features in the spectrum have a full width at half maximum of about 10 MHz. These are the central components of the angular momentum manifolds that are least sensitive to variations in the applied electric field. The broadest peaks have a full width at half maximum of around 40 MHz. These correspond to peaks that lie at the edge of the manifolds, which are more sensitive to electric fields and are broadened by small remaining stray electric fields and field inhomogeneities. The background in the spectrum results mainly from collisions between helium metastable atoms and background molecules ($H_2O$, $N_2$, and $O_2$, pressure in the vacuum chamber $\sim 10^{-7}$ mbar). A metastable helium atom can ionize a collision partner because of its high internal energy ($\sim 20$ eV). The resulting electrons can reach the electron multiplier and are counted. Their number was minimized by shielding the detection region. A residual background of approximately 8000 counts per second remained. In the experiments we averaged over every laser setting for 0.5 s. A typical count rate on one of the strong and narrow features is 30 000 counts per second.

To interpret the data in the framework of closed-orbit theory the spectra were Fourier transformed with respect to $F^{-1/4}$. For this procedure about ten laser scans were combined to obtain sufficient resolution in the Fourier spectra. In Figs. 3(d), 5(c), and 6(c) the Fourier transformed experimental spectra for $\epsilon=-2.940(4)$, $\epsilon=-2.350(4)$, and $\epsilon=-1.760(4)$, respectively, are plotted. The widths of typical peaks in the $\epsilon=-2.940(4)$, $\epsilon=-2.350(4)$, and $\epsilon=-1.760(4)$ action spectra in units of scaled action are 0.07, 0.04, and 0.05, respectively. The noise at low scaled action in each recurrence spectrum is an artifact and results from the slightly varying backgrounds in the scans that were combined to form the frequency spectrum. The spectra display a group structure with the individual groups being clearly visible, especially at $\epsilon=-2.940(4)$. At higher scaled energies the individual groups start to overlap at low action values.

### B. Comparison with closed-orbit theory

In Fig. 3(a) a closed-orbit calculation for hydrogen at $\epsilon=-2.940$ is shown. The calculated spectrum consists of groups of peaks. All orbits were created in bifurcations from the uphill orbit or one of its repeated traversals [along the positive $z$ axis ($u$ axis)] as the scaled energy decreases. Immediately following the bifurcation, the initial angle of the newly created orbit is almost zero (the initial angle of the uphill orbit). As the scaled energy is decreased further, the initial angle of the new orbit increases until it is equal to 180° (the initial angle of the downhill orbit), at which point it is absorbed and destroyed by the downhill orbit or one of its repeated traversals [along the negative $z$ axis ($v$ axis)] in an inverse bifurcation. Closed orbits can be distinguished by a rational number $m/n$. An $m/n$ orbit is born at a bifurcation of the $n$th repeated traversal of the uphill orbit and will be destroyed by the $m$th repeated traversal of the downhill orbit. An electron traveling along such an orbit will cross the $u$ axis $m$ times and the $v$ axis $n$ times before it exactly closes at the core. The first group in the recurrence spectrum corresponds to orbits with $n=m+1$, the next with $n=m+2$, and

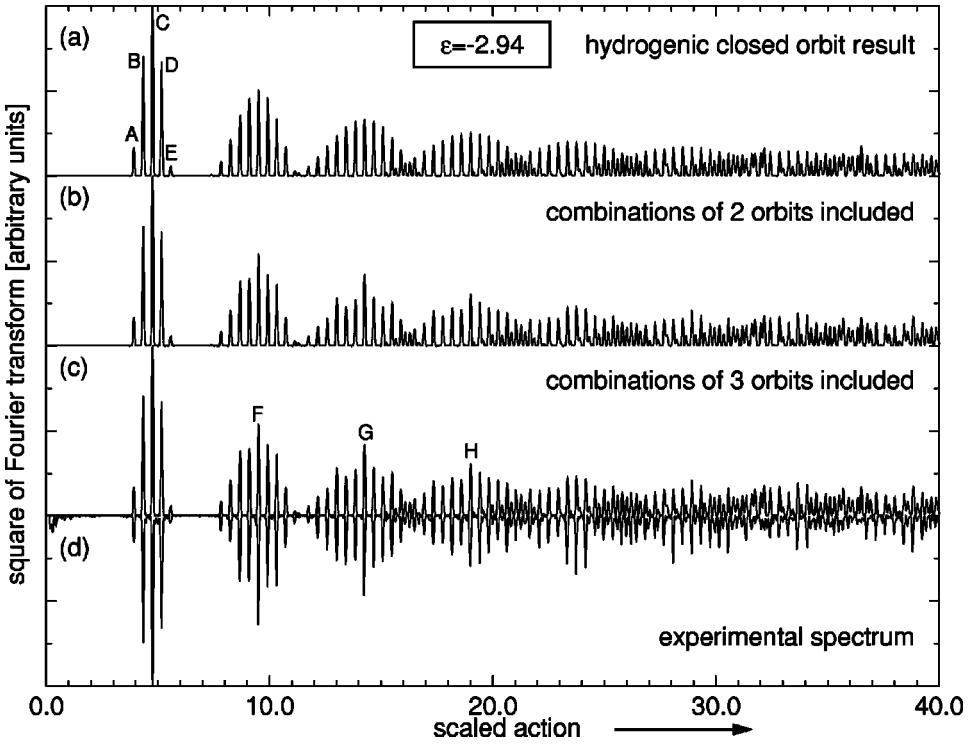


FIG. 3. Experimental Fourier transformed spectrum at $\epsilon=-2.940(4)$ compared with closed-orbit calculations for $\epsilon=-2.940$. (a) Calculation for hydrogen. (b) Calculation for helium including only sum orbits consisting of two hydrogenic orbits. (c) Calculation for helium including sum orbits up to combinations of three hydrogenic orbits. (d) Fourier transformed experimental spectrum.

so on. The increase of the initial launching angle as the scaled energy decreases is shown for the 9/10 orbit in the paper by Courtney *et al.* [5]. In Fig. 4 the orbits corresponding to the first five peaks in the action spectrum, indicated by $A-E$ in Fig. 3(a), are shown both in $(u,v)$ and in the more familiar $(\rho,z)$ coordinates. From their initial angle, it is clear that the 13/14 orbit on the right-hand side of the first group was just created, while the 9/10 orbit on the left-hand side will soon be destroyed. Since we investigated the $|M|=1$ case, orbits starting perpendicularly to the field direction give the strongest features in the action spectrum. At and close to the (inverse) bifurcation energy, orbits do not have intensity since their initial angle is almost (anti)parallel to the electric-field direction. Therefore, the uniform approximation derived by Gao and Delos for an atom in an electric field [15] is not required in $|M|=1$ spectra.

The calculated spectrum in Fig. 3(a) has to be compared with the experimental spectrum in Fig. 3(d). The agreement is already quite good, as might be expected since the quantum defects for $l\geqslant 1$ series in singlet helium are small. Deviations in the positions of the peaks may result from the uncertainty in the scaled energy. This can explain deviations in action of around $\pm 0.004$ for peaks in the first group and of around $\pm 0.008$ for those in the second group. Furthermore, small deviations in the positions may originate from the fact that we used $l_z=0$ for the calculation in the classical region. However, the maximum deviation in peak position up to $\tilde{S}=40$ is only 0.009, which is smaller than their linewidths in the recurrence spectra. Hydrogenic closed-orbit theory thus explains all peak positions. Differences mainly appear in the intensities of the peaks. In Figs. 3(b) and 3(c) the results of a closed-orbit calculation for helium are shown. Only the $l=1$ quantum defect was taken into account to save computer time (using higher-$l$ quantum defects did not significantly influence the calculation). In Fig. 3(b) only core-scattered terms resulting from combinations of two hydrogenic orbits were included; in Fig. 3(c) combinations of three hydrogenic orbits were included as well. Including the combinations of three hydrogenic orbits did not change the result significantly up to action 40 [compare Figs. 3(b) and 3(c)]. The inclusion of core effects, however, did improve the agreement between the experimental spectrum and closed-orbit theory considerably [compare Fig. 3(d) with Figs. 3(a) and 3(c)].

Adding core scattering mainly changes the intensity of peaks that are already present in the hydrogenic spectrum. This results from the fact that the spectrum consists of groups with almost equidistant peaks. Combinations of orbits from the first group therefore coincide with orbits from the second group. Furthermore, a combination of an orbit from

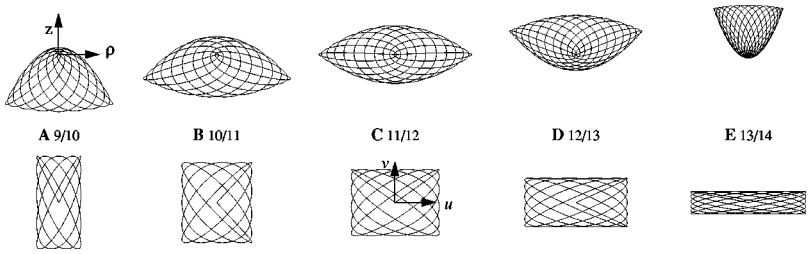


FIG. 4. Orbits corresponding to the first five peaks ($A$, $B$, $C$, $D$, and $E$) in the action spectrum for $\epsilon=-2.940(4)$ [Fig. 3(a)].

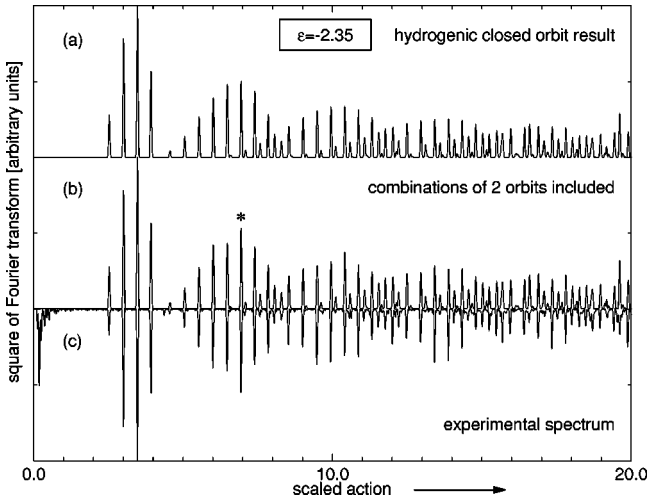


FIG. 5. Experimental Fourier transformed spectrum at $\epsilon=-2.350(4)$ compared with closed-orbit calculations for $\epsilon=-2.347$. (a) Calculation for hydrogen. (b) Calculation for helium including only sum orbits consisting of two hydrogenic orbits. (c) Fourier transformed experimental spectrum.

the first group with one from the second group coincides with orbits from the third group and so on. Because of this structure of the spectrum, core effects are visible only in the intensities, in contrast to the magnetic-field case where extra peaks occur [7]. As an example consider the fifth peak in the second group, which is indicated by an *F* in Fig. 3(c). It is the first harmonic of peak *C* in the hydrogenic case. Adding core scattering, combinations of peak *B* and peak *D* and of peak *A* and peak *E* and a combination that is twice peak *C* contribute to its intensity change (an increase or a decrease depending on the relative phases of the contributions). Similar reasoning results in increased intensities for the peaks *G* and *H* in Fig. 3(c). Small deviations with theory in the intensities of peaks *B* and *D* can be understood within the error margin of the scaled energy. The agreement up to scaled

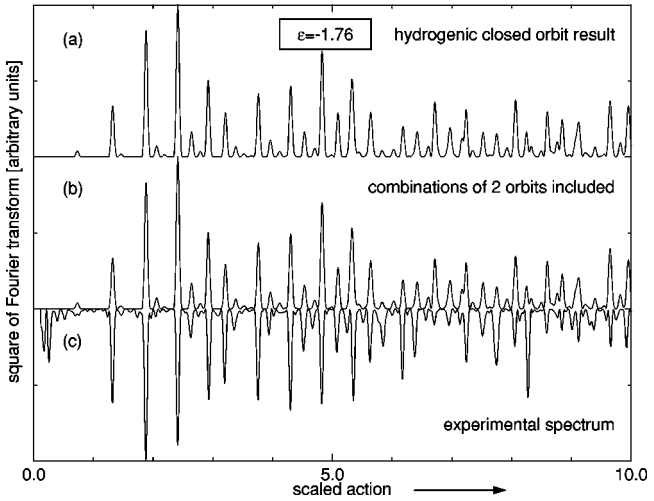


FIG. 6. Experimental Fourier transformed spectrum compared with closed-orbit calculations for $\epsilon=-1.760$. (a) Calculation for hydrogen. (b) Calculation for helium including only sum orbits consisting of two hydrogenic orbits. (c) Fourier transformed experimental spectrum.

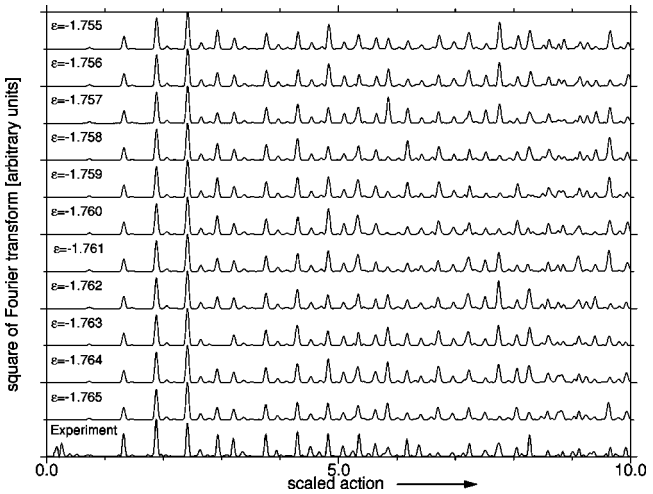


FIG. 7. Hydrogenic closed-orbit calculations at some scaled energy values around $\epsilon=-1.760$.

actions of around 30 now is very good. Closed-orbit theory in which core scattering is included predicts the correct peaks to gain intensity. This increase is slightly smaller than that observed experimentally. To our knowledge, this is the best agreement (up to the highest action) achieved so far between an experimental spectrum below the saddle point and a closed-orbit calculation.

In Fig. 5(a) a hydrogenic closed-orbit calculation at $\epsilon=-2.347$ is shown. This scaled energy value is chosen since it shows the best agreement with the experimental spectrum recorded at $\epsilon=2.350(4)$. Again deviations between the calculation and the experimental spectrum in Fig. 5(c) occur mainly in the intensities of the peaks. Deviations in positions are comparable with those in the $\epsilon=-2.940$ case. In Fig. 5(b) the result of a calculation for helium, including core-scattered terms resulting from combinations of two hydrogenic orbits, is shown. We find good agreement in this case for actions up to approximately 20. A clear example of the improvement achieved by including core effects is seen in the gain of intensity in the peak at action 6.937 (indicated with an asterisk).

In Fig. 6 the spectrum at $\epsilon=-1.760(4)$ is compared with closed-orbit theory. In Fig. 6(a) the calculation for hydrogen is shown. Up to action 6 the agreement between this calculation and the experimental spectrum in Fig. 6(c) is reasonably good. Calculations for helium are shown in Fig. 6(b). The hydrogenic and helium closed-orbit calculations do not differ much, so there is little improvement gained by including the core in this case. Since the agreement between theory and experiment diminishes for higher scaled energy, calculations at values around $\epsilon=-1.760$ were performed to study the sensitivity of the spectrum for small changes in the value of $\epsilon$ (allowed by the experimental accuracy). The results of this procedure are shown in Fig. 7. For lower scaled action ($\tilde{S}<5.0$), where the experiment agrees reasonably with the closed-orbit calculation, the calculation is insensitive to the value of the scaled energy. At higher actions the sensitivity increases rapidly and many peaks show a strong dependence on the precise value of the scaled energy. However, a better value for $\epsilon$ that explains all deviations simultaneously within

the estimated stability range of 0.001 for the scaled energy was not found. The reason for these residual deviations remains unclear.

## V. CONCLUSIONS

We performed scaled-energy experiments on helium $M=\pm 1$ Rydberg atoms (singlet series) in an electric field. These experiments have high frequency resolution, which allows for investigation of the high action part of the recurrence spectra. The long energy range over which the spectra were recorded also resulted in the good resolution in the recurrence spectra. We interpreted our data using closed-orbit theory. Agreement between theory and experiment is almost perfect at the lower scaled-energy values we investigated when effects of core scattering are included. Towards higher scaled energies the agreement becomes less good. Here the recurrence spectra are more sensitive to the precise value of the scaled energy. The deviations between experiment and closed-orbit theory, however, cannot be attributed solely to the sensitivity on the exact value of the scaled energy. The lesser agreement for higher scaled energy suggests that tunneling through and/or scattering over the saddle in the potential might be important. These effects were not incorporated in our implementation of closed-orbit theory.

We plan to present experiments on $M=0$ Rydberg states in a subsequent paper. In these spectra the parallel and antiparallel (to the applied field direction) orbits are present and the behavior around bifurcations can be studied. Furthermore, $M=0$ spectra are expected to display stronger core effects since the large $^1S$ quantum defect has to be considered.

## ACKNOWLEDGMENTS

We thank J. Bouma for his excellent technical assistance and D. Delande for performing quantum calculations around $\epsilon=-3$. P.A.D. thanks the EPSRC for funding and T.S. Monteiro for helpful discussions.

[1] J. Gao and J. B. Delos, Phys. Rev. A **49**, 869 (1994).
[2] J. Gao, J. B. Delos, and M. Baruch, Phys. Rev. A **46**, 1449 (1992).
[3] J. Gao and J. B. Delos, Phys. Rev. A **46**, 1455 (1992).
[4] U. Eichmann, K. Richter, D. Wintgen, and W. Sandner, Phys. Rev. Lett. **61**, 2438 (1988).
[5] M. Courtney, N. Spellmeyer, H. Jiao, and D. Kleppner, Phys. Rev. A **51**, 3604 (1995).
[6] G. J. Kuik, A. Kips, W. Vassen, and W. Hogervorst, J. Phys. B **29**, 2159 (1996).
[7] D. Delande, K. T. Taylor, M. H. Halley, T. van der Veldt, W. Vassen, and W. Hogervorst, J. Phys. B **27**, 2771 (1994).
[8] Quantum calculations performed by D. Delande.
[9] T. S. Monteiro and G. Wunner, Phys. Rev. Lett. **65**, 1100 (1990).
[10] G. Raithel, H. Held, L. Marmet, and H. Walther, J. Phys. B **27**, 2849 (1994).
[11] P. A. Dando, T. S. Monteiro, D. Delande, and K. T. Taylor, Phys. Rev. Lett. **74**, 1099 (1995).
[12] P. A. Dando, T. S. Monteiro, D. Delande, and K. T. Taylor, Phys. Rev. A **54**, 127 (1996).
[13] B. Hüpper, J. Main, and G. Wunner, Phys. Rev. Lett. **74**, 2650 (1995).
[14] B. Hüpper, J. Main, and G. Wunner, Phys. Rev. A **53**, 744 (1996).
[15] J. Gao and J. B. Delos, Phys. Rev. A **56**, 356 (1997).